Research Article

Hassan Alipour, Ali Hamedani, and Ghasem Alahyarizadeh*

First-principles calculations to investigate the thermal response of the $ZrC_{(1-x)}N_x$ ceramics at extreme conditions

https://doi.org/10.1515/htmp-2022-0241
received May 25, 2022; accepted September 12, 2022

Abstract: We present the thermodynamic properties of $ZrC_{(1-x)}N_x$ ceramics at elevated temperature (0–1,000 K) and pressure (0–150 GPa) conditions, explored by density functional theory. We implemented the Debye–Grüneisen quasi-harmonic model in our calculations. In our investigation, we cover elastic constants, elastic moduli, compressibility, ductility/brittleness, hardness, sound velocities, minimum thermal conductivity, melting temperature, anisotropy indices, isothermal bulk modulus, heat capacities, entropy, Debye temperature, Grüneisen parameter, thermal expansion coefficient, and thermal pressure. We address the effect of the structural anisotropy and bonding nature of $ZrC_{(1-x)}N_x$ compounds on their thermal response to extreme conditions. Considering $ZrC_{(1-x)}N_x$ with the x in the range of 0.0, 0.25, 0.5, 0.75, and 1.0, $ZrC_{0.50}N_{0.50}$ stands out in the response to the applied conditions. At higher temperatures, the thermal expansion of the $ZrC_{0.50}N_{0.50}$ shows a smaller increase, which makes it a favorable candidate for coating material in cutting tools against commonly used ZrN and ZrC ceramics. Similar behavior is observed for the heat capacity by increasing pressure at higher temperatures, where a smaller reduction is observed. It could be interpreted as a more stable response regarding the application-specific design conditions.

Keywords: thermodynamic properties, DFT, $ZrC_{(1-x)}N_x$, high pressure, high temperature

1 Introduction

Over the past two decades, transition metal carbides (TMCs) and transition metal nitrides (TMNs) have been utilized in various technological applications due to their appealing properties such as excellent mechanical stability, hardness, conductivity, and erosion resistance. Drill bits, golf shoe spikes, and snow tires are examples of the applications where their remarkable mechanical properties come into play. Their interesting electronic, optical, and magnetic properties have also given them applications in manufacturing optoelectronic devices, such as electrical contacts and optical coatings [1]. In addition, the excellent catalytic activity of TMCs makes them a proper choice for applications where higher electrochemical performance is demanded [2]. The interesting properties of TMCs and TMNs originate from their peculiar bonding nature; their structures contain covalent, metallic, and ionic bonds [3–6].

Zirconium carbide (ZrC) and zirconium nitride (ZrN) are two widely used TMCs and TMNs that meet the strict requirements of different industrial applications. Owing to their hardness and good resistance at high pressure and high temperature conditions, they are commonly used in manufacturing cutting tools, tool bits, and machinery [7]. Rock-salt structure is the ground state structure of ZrC and ZrN ceramics, a crystalline face-centered cubic (FCC) structure with the *Fm3m*-225 space group [8]. In this structure, carbon and nitrogen are located in the octahedral interstitial positions. The structure contains covalent, metallic, and ionic bonds, among which the covalent bonds are the dominant type.

Vibrational thermal effects are essential in the calculation of the thermodynamic properties of a solid as a function of pressure and temperature, $f(p, T)$ [9]. This function can be represented through Debye–Grüneisen quasi-harmonic model that provides vibrational Helmholtz free energy under given conditions [10]. Equation of states (EOSs) is then obtained by minimizing non-equilibrium Gibbs free

* **Corresponding author: Ghasem Alahyarizadeh,** Faculty of Engineering, Shahid Beheshti University Tehran, Iran, e-mail: g_alahyarizadeh@yahoo.com, tel: +98 21 29904223
Hassan Alipour, Ali Hamedani: Faculty of Engineering, Shahid Beheshti University Tehran, Iran

energy at arbitrary temperatures and pressures [11,12]. Thermodynamic properties provide insight into the atomic interactions, interatomic bond strength, and stability of the alloys, properties that are affected by the lattice vibrations [13–15].

The thermodynamic characteristics of ZrC and ZrN have been extensively investigated, both experimentally and theoretically. X-ray radiation, ultrasonic and electromotive force, Knudsen cell, differential thermal analysis, cryostat, and calorimeter are among the experimental methods implemented to better understand these materials' behaviors under extreme conditions [3,8,16]. *Ab initio* and classical molecular dynamics are theoretical methods that provide an atomic-level description of the underlying physics. This feature can describe and justify the experimental observations or even build a predictive model. First-principles calculations, developed based on the pseudopotential and full potential approaches, are broadly used in physics, mechanics, and materials science to calculate a wide range of material properties. In context with these powerful simulation tools, various theoretical models, such as the augmented plane wave method [17,18], muffin-tin orbital techniques [17,19,20], and their linearized versions, the linearized augmented-plane-wave (LAPW) and the linear muffin-tin orbital, have been developed [17,19,21]. Moreover, different approximations, such as local density approximation (LDA) [22], generalized gradient approximation (GGA) [23], or Perdew, Burke, and Ernzerhof for solid (PBEsol) [24], have been developed in the framework of the density functional theory (DFT) method [25].

Numerous studies have been conducted to investigate the thermodynamic properties of ZrC and ZrN. Guillermet et al. analyzed the available thermodynamic information and calculated the cohesive energy of carbides and nitrates of 4d metals. They reached an order of precision that made a detailed comparison between *ab initio* and experimental results became possible [26]. Using the first-principles calculations, Hao et al. calculated various features of ZrC and ZrN, including pressure-induced structure transition, elastic constants, heat capacity, and Debye temperature as a function of temperature and pressure [27]. Zhu et al. examined the elastic and thermodynamic properties of ZrC by *ab initio* pseudopotential plane-wave calculations. They also used quasi-harmonic Debye models to calculate the temperature/pressure dependence of some of these elastic and thermodynamic properties [6]. Kim et al. studied the temperature- and pressure-dependent thermodynamic properties of ZrC, ZrN, and $ZrC_{0.50}N_{0.50}$ using first-principles calculations and Debye–Grüneisen theory. They concluded that except for the bulk modulus, $ZrC_{0.50}N_{0.50}$ has the highest elastic moduli [28]. Jing et al. provided a combination of the quasi-harmonic Debye model and thermal electronic excitation to study the thermodynamic properties of ZrC for the stable rock-salt structure. One of their quantitative results was that below the critical point of $V/V_0 = 0.570$, the transition of the B1 to B2 structure has the highest probability at higher pressures [29]. Varshney and Shriya presented the thermodynamic properties of some TMCs at high pressure and temperature within the framework of a quasi-harmonic Debye model. They reported that the heat capacity decreases nonlinearly with the applied pressure at different temperatures [30]. Yang et al. studied the thermodynamic properties of different transient metal carbides and nitrides with DFT based on the quasi-harmonic Debye–Grüneisen model. One of their reported results is that carbides and nitrides have higher heat capacity at higher pressure and temperature than metals [31]. Using the full-potential LAPW (FP-LAPW) method, implemented in WIEN2k, various properties of materials, including electronic, thermoelectric, optical, mechanical, magnetic, and magneto-electronic properties of different materials, were investigated in the literature [32–43]. Although a few studies have addressed the thermodynamic properties of ZrN and ZrC at elevated pressures and temperatures, little attention has been paid to the comparative study of the thermodynamic properties of their ternary compounds. In this article, we perform first-principles calculations using the FP-LAPW method to study the structural and mechanical properties and the temperature- and pressure-dependence of the thermodynamic properties of ZrC, ZrN, and their ternary compounds, $ZrC_{(1-x)}N_x$. We elucidate how the bonding in $ZrC_{(1-x)}N_x$ structure affects its properties. As for the mechanical properties, we cover elastic constants, bulk, shear, and Young's moduli, compressibility, Poisson's ratio, Cauchy pressure, Pugh's ratio, and hardness. We also explore different thermodynamic properties in our investigation, including sound velocities, minimum thermal conductivity, melting temperature, anisotropy indices, isothermal bulk modulus, heat capacities, entropy, Debye temperature, Grüneisen parameter, thermal expansion coefficient, and thermal pressure. Our results could facilitate selecting the $ZrC_{(1-x)}N_x$ compound, from which a superior response is expected in the given harsh conditions. In addition, our results could provide a theoretical basis for the experimental investigations. By investigating a range of C and N concentrations, we show how structural properties could be manipulated to achieve the desired outcomes in a specific application. The structure of the article is as follows. After presenting the computational details in Section 1, we describe the theoretical basis of the calculated properties in

Section 2. Results and the associated discussion are presented in Section 3. Section 4 contains the conclusion and outlook.

2 Computational details

DFT calculations were performed in the FP-LAPW framework as implemented in the WIEN2k package [19,44,45]. The PBE GGA exchange-correlation functional [44] was used in all simulations. The wave function inside the muffin-tin spheres was extended as spherical harmonics, for which the maximum angular momentum was considered to be l_{max} = 10. The proper convergence was obtained by setting the plane wave cutoff for kinetic energy as $R_{MT}K_{max}$ = 7. The expansion of the plane wave outside of the sphere is called the interstitial region. The convergence of the total energy and zero charge leakage from particles was considered in the configuration of the muffin-tin radiuses (R_{MT}) [32]. The R_{MT} values for C, N, and Zr atoms were set to 1.89, 1.94, and 2.31, respectively. The convergence criterion in self-consistent calculations is the energy convergence with the tolerance of 10^{-4} Ry. The experimental lattice parameter of ZrC was initially used to create its crystal structures. The ternary $ZrC_{(1-x)}N_x$ compounds, x being 0.25, 0.5, 0.75, and 1, were built by substituting the corresponding number (to x) of C atoms with N atoms. After structure minimization, the optimum lattice constants were obtained, and the structures were rebuilt to be used in the calculations. It should be noted that due to the existence of different bonds and deviation from cubic symmetry, ternary structures have anisotropy similar to the orthorhombic structure, and they took different a, b, and c values upon optimization. Moreover, 5,000 k-points were used for sampling the Brillouin zone. As mentioned earlier, the Bravais lattice of ZrC and ZrN crystals is a FCC known by the Fm-3m structural group. In order to create structures with the desired content of N and C atoms, a $1 \times 1 \times 1$ cell containing four Zr atoms and four C or N atoms was created. Monitoring energy-vs-volume was used to obtain the optimized lattice parameter and bulk modulus. The structure with lower internal energy was taken as the stable structure. The elastic constants were calculated using the IRelast package [46], and the Voigt–Reuss–Hill (VRH) approximation was used to account for the polycrystalline elasticity (elastic moduli) at zero pressures [37,41]. In addition, the thermodynamic parameters were calculated using the Debye–Grüneisen quasi-harmonic model [47] as implemented in the Gibbs2 package [11,48]. Based on the obtained results, the temperature range of 0–1,000 K (the temperature near the Debye temperature) and pressure range of 0–150 GPa (the pressure at which the structures are still stable in their phases) were considered for the representation of all thermal parameters.

2.1 Equilibrium structure and mechanical properties

The energy–volume relationship is an isothermal EOS describing the thermodynamic correlation of energy, pressure, and volume at a constant temperature. One of the EOSs widely used to estimate the optimum volume against energy is the Birch–Murnaghan (B–M) isothermal equation. This equation is derived by taking the relationship between the volume of the crystal and the applied pressure into account. B–M isothermal equation describes the system's internal energy as a function of volume as in the following equation (1):

$$E(V) = E_0 + \frac{9V_0B_0}{16}\left\{\left[\left(\frac{V_0}{V}\right)^{\frac{2}{3}} - 1\right]^3 B_0' + \left[\left(\frac{V_0}{V}\right)^{\frac{2}{3}} - 1\right]^2\left[6 - 4\left(\frac{V_0}{V}\right)^{\frac{2}{3}}\right]\right\}. \quad (1)$$

Here, E is internal energy, V_0 is the volume of the reference structure, V is the volume of the deformed structure, B_0 is the bulk modulus, and B_0' is the pressure derivative of the bulk modulus. In experimental studies, the bulk modulus and its derivative are usually obtained by fitting this equation to the available data points. In theoretical studies, however, this equation is acquired by finding the best fit to the energy of structures in a predefined range of system volume (i.e., by deforming the cell) [49].

Different parameters were taken into account to investigate the mechanical behavior of the structure. First, we calculated the elastic moduli (bulk, shear, and Young's modulus) using the VRH approximations, which establish a relationship between the elastic constants of anisotropic single crystalline and isotropic polycrystalline elastic moduli [7]. The brittle or ductile nature of $ZrC_xN_{(1-x)}$ structures was described by evaluating the Poisson's ratio, the Pugh's ratio, and the Cauchy pressure, based on the method introduced in ref. [50]. In addition, the hardness, the sound velocities, the minimum thermal conductivity, the melting temperature, and the anisotropy indices of $ZrC_xN_{(1-x)}$ were calculated using the corresponding relations

explained in refs [21,50,51]. All the mechanical parameters were calculated at atmospheric pressure.

2.2 Thermodynamic parameters

A solid's thermodynamic properties are related to its lattice's phonon vibrations. Calculating these properties at high temperatures and pressures can help us better understand how they behave in environments with extreme conditions. This work explores different thermodynamic properties, including isothermal bulk modulus, specific heat capacities (at constant pressure and volume), entropy, Debye temperature, Grüneisen parameter, thermal expansion coefficient, and thermal pressure. We chose a range of temperature and pressure at which the Debye–Grüneisen quasi-harmonic model is valid. This model extends the framework of harmonic phonons to high temperatures by considering the effects of thermal expansion against a bulk modulus.

Further information about this model can be found elsewhere [52]. Therefore, by implementing this model, phonon vibrations at high temperature/pressure conditions are considered. This provides better resolution in quantifying how thermodynamic properties are affected in extreme conditions [11,52]. The Gibbs non-equilibrium function obtained from this model is expressed in equation (2) as follows:

$$G^*(V;P,T) = E(V) + PV + F_{\text{vib}}[\theta_{\text{D}}(V), T], \tag{2}$$

where $E(V)$ is internal energy per unit cell, $P(V)$ is constant hydrostatic pressure, T is temperature, and $\theta(V)$ is Debye temperature. F_{vib} is the vibrational Helmholtz free energy, which is related to the phonon vibrations through the Debye model and is defined in equation (3) as follows [53]:

$$F_{\text{vib}}(\theta_{\text{D}}, T) = nk_{\text{B}}T\left[\frac{9\theta_{\text{D}}}{8T} + 3\ln\left(1 - e^{-\frac{\theta_{\text{D}}}{T}}\right) - D\left(\frac{\theta_{\text{D}}}{T}\right)\right]. \tag{3}$$

In equation (3), k_{B} is the Boltzmann constant, $D(\theta_{\text{D}}/T)$ is the Debye function, and n is the number of atoms per unit cell. Debye temperature, θ_{D}, is also an important thermophysical property that reflects the phonon contributions to the entropy and provides a reasonable estimation of the vibrational entropy [52]. This property is related to a solid's maximum frequency of thermal vibration, in which the corresponding wavelength equals the lattice constant [54]. It is known that the Debye temperature is also a reflection of the strength of the chemical bonding and the hardness of materials. So, in some sense, the Debye temperature indicates the rigidity of the material, i.e., the higher the Debye temperature, the harder the material (stronger covalent bonds and greater hardness/rigidity) [28,31,55]. The Debye temperature (θ_{D}) generally relates to properties like lattice vibration, specific heat, thermal conductivity, melting temperature, thermal expansion coefficient, and elastic constants. Therefore, it is an essential property for describing well-known phenomena in solid-state physics [56,57]. Increasing the number of constituent elements of the structure can also lead to an alternation in Debye temperature, which could be inferred as a variation of the material's rigidity [58]. Debye temperature is usually obtained empirically from heat capacity measurements. However, since acoustic vibrations are the only source of vibrational excitations at low temperatures, the Debye temperature is theoretically calculated from elastic constants. This is the same as its determination from specific heat capacity measurements [30,52]. Since the velocity of the elastic waves, which propagate through the lattice, can be determined from elastic constants, the Debye temperature can also be correlated with the elastic constants [52]. For an isotropic solid, equation (4) describes the Debye temperature in terms of system volume $\theta_{\text{D}}(V)$ as follows [59]:

$$\theta_{\text{D}} = \frac{\hbar}{k_{\text{B}}}[6\pi^2V^{1/2}]^{1/3}f(\sigma)\sqrt{\frac{B_s}{M}}, \tag{4}$$

where M is the atomic mass per unit cell, $\hbar$ is the plank constant, σ is Poisson's ratio, and B_{s} is the adiabatic bulk modulus, approximated at the equilibrium atomic volume V_0 by equation (5) as follows [11]:

$$B_S \approx B(V) = V\left(\frac{d^2E(V)}{dV^2}\right). \tag{5}$$

Also, the value of $f(\sigma)$ is calculated in terms of Poisson's ratio as in equation (6) [11].

$$f(\sigma) = \left\{3\left[2\left(\frac{2}{3}\frac{1+\sigma}{1-2\sigma}\right)^{3/2} + \left(\frac{1}{3}\frac{1+\sigma}{1-\sigma}\right)^{3/2}\right]^{-1}\right\}^{1/3}. \tag{6}$$

By deriving the non-equilibrium Gibbs function as a function of volume, the thermal EOS as a function of temperature and pressure can be obtained. We used Gibbs2 code to explore the temperature and pressure dependence of the thermodynamic properties of the target ZrC, ZrN, and $ZrC_{(1-x)}N_x$ materials. This code uses the quasi-harmonic approximation to quantify this dependency. As a result, several thermodynamic parameters can be obtained by specifying the equilibrated volume and thermal EOS that are presented later [11].

2.2.1 Isothermal bulk modulus

Investigating the behavior of bulk modules at different temperatures and pressures provides an understanding of the thermoelastic and non-harmonic properties of a crystal [31]. Isothermal bulk modulus (B) is an intensive property, having a constant value at the normal ambient condition. It is viewed as a manifestation of the elastic response of a solid to the hydrostatic compression or, in other words, resistance to the volume change [60]. This parameter is one of the basic quantities that determines the elasticity of an isotropic material and is usually used to estimate the structural strength of the material. As an important engineering parameter, bulk modulus has intimate relation with the performance characteristics of a material, e.g., the expansibility, elasticity, Debye temperature, thermal conductivity, elastic wave velocity, and heat capacity. A higher bulk modulus in a mechanically stiffened material is related to the compression and strengthening of bonds or, lower lattice vibrations. In fact, the pressure-induced stiffening of the material is ascribed to an increased cohesive energy. Hence, bulk modulus can be tuned by applying pressure and temperature [61]. Using the proposed EOS, the behavior of the isothermal bulk modulus at different temperatures can be obtained from equation (7) as follows [37]:

$$B_T(P, T) = V\left(\frac{\partial^2 G^*(V;P, T)}{\partial V^2}\right)_{P,T}. \tag{7}$$

2.2.2 Entropy

Atomic properties such as atomic size and mass, electron-to-atom ratio, and electronegativity are often used to justify the vibrational entropy profile since subatomic particles such as electrons also contribute to the vibrational entropy of solids. Variation of interatomic force constants due to the temperature change can explain the dependence of the vibrational entropy on the temperature (at constant volume) [31]. In the quasi-harmonic approximation, the vibrational entropy of the crystal (S) in conditions far from phase transition is calculated from equation (8) as follows [62]:

$$S = -3nk_{\mathrm{B}} \ln\left(1 - e^{\frac{-\theta_{\mathrm{D}}}{T}}\right) + 4nk_B D\left(\frac{-\theta_{\mathrm{D}}}{T}\right). \tag{8}$$

2.2.3 Grüneisen parameter

The Grüneisen parameter, denoted by γ, describes the effect of the volume change of the lattice on its vibrational properties. So, it reflects the anharmonic effects on the properties of the solid and could represent the effects of temperature/pressure change on the atomic displacements and dynamics of the lattice [63]. Any change in the lattice vibration that comes from variations in temperature or pressure (which eventually results in volume change) can be described by the Grüneisen parameter [31,54]. For most solids, the Grüneisen parameter has a value of 1.5–2.5 [30]. This parameter is generally written as a dimensionless combination of thermal expansion coefficient, isothermal bulk modulus, density, and specific heat capacity. Therefore, it provides a qualitative relationship between the thermal and mechanical properties of the element, as expressed in equation (9) [64]:

$$\gamma = \frac{V}{C_{\mathrm{v}}}\left(\frac{\partial S}{\partial V}\right)_T = \frac{\alpha B_T V}{C_{\mathrm{v}}}. \tag{9}$$

2.2.4 Volumetric thermal expansion coefficient

An increase in temperature causes the atoms to vibrate at a higher frequency (in higher energy states), giving rise to the higher contribution of vibration-related anharmonic behavior. This could also be related to the variation of interatomic distances, as energetic atoms can move further from each other. Bonding strength determines the extent to which the atoms can oscillate; the stronger the bonds, the lower the thermal expansion, and *vice versa* [65]. When heating a ceramic whose constituent elements have different thermal expansions, crack generation will be unavoidable [8]. This is a challenge in many technological applications, like thin film coatings and cutting tools. A mismatch of the thermal expansions generates thermal stresses at the interface of the two materials and reduces their adherence to the substrate [31]. Taking the definition of the thermal expansion coefficient (α) into consideration (equation (10)), any expansion/contraction of the lattice due to the variation of the temperature causes the frequency of the vibrations to change [30]. Although the value of thermal expansion has a directional dependency in the crystal, this parameter can also be considered to be isotropic by the assumption of isotropic structure (single crystal with cubic symmetry). Isotropic thermal expansion can be obtained from equation (10). It is also worth noting that there is a similarity between the temperature dependence of the thermal expansion coefficient and specific heat capacity in the crystals as follows [65]:

$$\alpha = -\frac{1}{V}\left(\frac{\partial V}{\partial T}\right)_{\mathrm{p}} = \frac{\gamma C_{\mathrm{v}}}{VB_T}, \tag{10}$$

2.2.5 Heat capacity

Heat capacity plays a vital role in linking thermodynamics with lattice dynamics. The knowledge of the material's specific heat capacity provides an insight into its vibrational properties [31]. Heat capacity correlates with the amount of thermal energy added to the material and the resulting temperature change. Increasing the heat capacity upon rising the temperature implies phonon thermal softening in the structure [66]. Einstein's formula [67], derived from the vibration of the molecular bonds, provides a reasonable estimation of the heat capacity. According to this relation, heat capacity reaches zero as T approaches 0 K, and at sufficiently low temperatures, it is proportional to T^3 [68]. At high temperatures, heat capacity reaches a saturation plateau, the Dulong–Petit limit, which is caused by the energy saturation of oscillating bonds [8,69]. In addition, the heat capacity of materials decreases non-linearly with pressure at different temperatures, meaning that the vibration frequency of the particles in materials is influenced by temperature and pressure. However, heat capacity varies weakly with pressure for higher temperatures, e.g., close to the Debye temperature [30]. Equations (11) and (12) describe the heat capacity at constant pressure (C_p) and the heat capacity at constant volume (C_v) as a function of temperature and show the interconnection of these parameters as follows [69]:

$$C_v = 12nk_B D\left(\frac{\theta_D}{T}\right) - 9nk_B\frac{\theta_D}{T}\left(\frac{1}{e^{\frac{\theta_D}{T}} - 1}\right), \tag{11}$$

$$C_p = \left(\frac{\partial H}{\partial T}\right)_p = C_v(1 + \gamma\alpha T). \tag{12}$$

2.2.6 Thermal pressure

Thermal pressure is a physical quantity important for investigating a material's thermoelastic properties at high temperatures [70]. Thermal pressure represents the expansion induced by the atomic vibrations and collective excitations of phonon vibrational modes in the crystal. The volumetric expansion of solids due to the temperature increase directly depends on that material's thermal pressure [71]. Having thermal pressure, an isothermal EOS can be converted to a temperature-dependent EOS. Thus, a more accurate EOS could be expected from a well-described thermal pressure as a function of temperature [72]. Thermal pressure is obtained from lattice dynamics and thermodynamics through a relationship that correlates thermal pressure, in an isobar condition, to the isothermal bulk modulus and thermal expansion [73]. From another point of view, thermal pressure is a measure of the pressure change resulting from temperature change at a constant volume [74]. Equation (13) provides thermal pressure derived by quasi-harmonic approximation as follows [75]:

$$p_{th} = \frac{\gamma}{V}\left[\frac{9}{8}nk_B\theta_D + 3nk_B TD\left(\frac{\theta_D}{T}\right)\right]. \tag{13}$$

3 Results

3.1 Structural and mechanical properties

Structural parameters of a crystalline material, such as its bulk modulus, its first pressure derivative, and equilibrium lattice constant, can be obtained via monitoring the system's total energy in a range of system volumes around the ground state. We calculated the total energy of $ZrC_{(1-x)}N_x$ structures with the x being 0, 0.25, 0.5, 0.75, 1. Then, the third-order Birch–Murnaghan EOS was fitted to the energy-volume data points. Table 1 compares the values of the properties obtained from our calculations with the experimental data and those reported in the literature. The values of the ground state energy (E_0) and corresponding volume (V_0), lattice constant (a), and the first pressure derivative of bulk modulus (B') are listed in Table 1. As seen, the lattice constants of the ternary ceramics differ slightly in three directions, indicating a slight deviation of these compounds from the symmetric cubic structure. Figure 1 presents a variation of the lattice constant for different nitrogen contents in the structure. As seen, a good agreement with ref. [76] has been acquired, but both the simulated results are ~0.03 off with respect to the experimental value. It should be noted that the experimental values are determined by the neutron scattering measurements. The elastic constants determined by this method have about (10–15%) uncertainty [77], which could be the reason for the discrepancy between the simulated and experimental results. Increasing the N content leads to a decrease in lattice constant and, subsequently, the volume of the structure; this trend is also shown as a function of temperature and pressure in Figure 2.

Mechanical properties of materials and the stability of their crystal structures can be perceived through the derivation of elastic constants, which for the cubic structure are only C_{11}, C_{12}, and C_{44} due to the structural symmetry. In Table 2, elastic constants (C_{ij}), elastic moduli (B, E, and G), compressibility (ρ), and ductility/brittleness criteria for ZrC and ZrN and their ternary ceramics are

Table 1: Volume (V_0), energy (E_0), and lattice constant of the ground state structure (a), the first pressure derivative of the bulk modulus (B) calculated from the Birch–Murnaghan equation and the experimental and other calculated theoretical values

	V_0 (Å^3)	B'	E_0 (Ry)	a (Å)	b (Å)	c (Å)
ZrC	104.8909	4.1162	−29,099	4.71605		
Expt.[a]				4.68		
Others (GGA)b				4.724		
Others (LDA)[c]				4.69		
$ZrC_{0.75}N_{0.25}$	102.9033	4.1828	−29,132	4.68599	4.68599	4.68626
Others[b]				4.699		
$ZrC_{0.50}N_{0.50}$	101.0927	4.0841	−29,166	4.65856	4.65854	4.65820
Others[b]				4.671		
$ZrC_{0.25}N_{0.75}$	99.29783	4.3817	−29,199	4.63083	4.63082	4.63048
Others[b]				4.642		
ZrN	97.74682	4.4624	−29,232	4.60649		
Expt.[d]				4.537		
Others (GGA)[b]				4.619		
Others (LDA)[e]				4.53		

a. Ref. [78]; b. Ref. [76]; c. Ref. [76]; d. Ref. [77]; and e. Ref. [78].

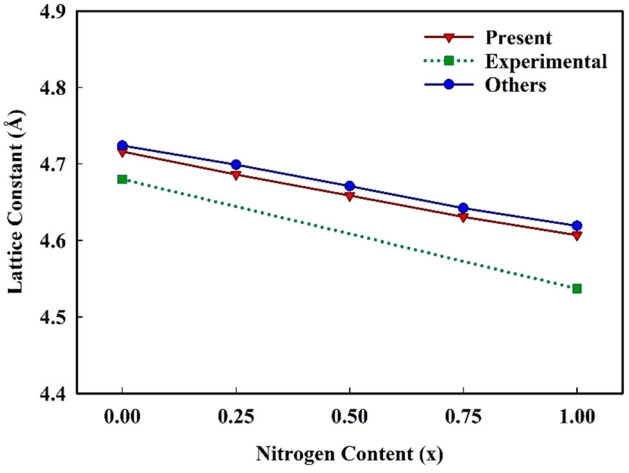

Figure 1: lattice constant of $ZrC_{(1-x)}N_{(x)}$ as a function of nitrogen content (x).

presented. An increase in N-content has various influences on the different elastic constants. Structural stability of the materials can be investigated by the Born mechanical stability criteria (for cubic structure: $C_{44} > 0$, $C_{11} + 2\,C_{12} > 0$, $C_{11} - C_{12} > 0$) [50], using the elastic constants. According to Table 2, all structures are mechanically stable. In the ternary compounds, increase in N-content leads to an increase in C_{11}, indicating the strengthening against the length change. The C_{12} value of $ZrC_{0.50}N_{0.50}$ indicates its highest resistance to the deformation resulting from the axial stress in the plane (100). On the other hand, $ZrC_{0.25}N_{0.75}$ has a higher resistance to deformation due to the applied tangential shear stress than the other ceramics; this is perceived from its C_{44} value. The calculated bulk modulus is 224.38 GPa, in a good agreement with the experimental value of

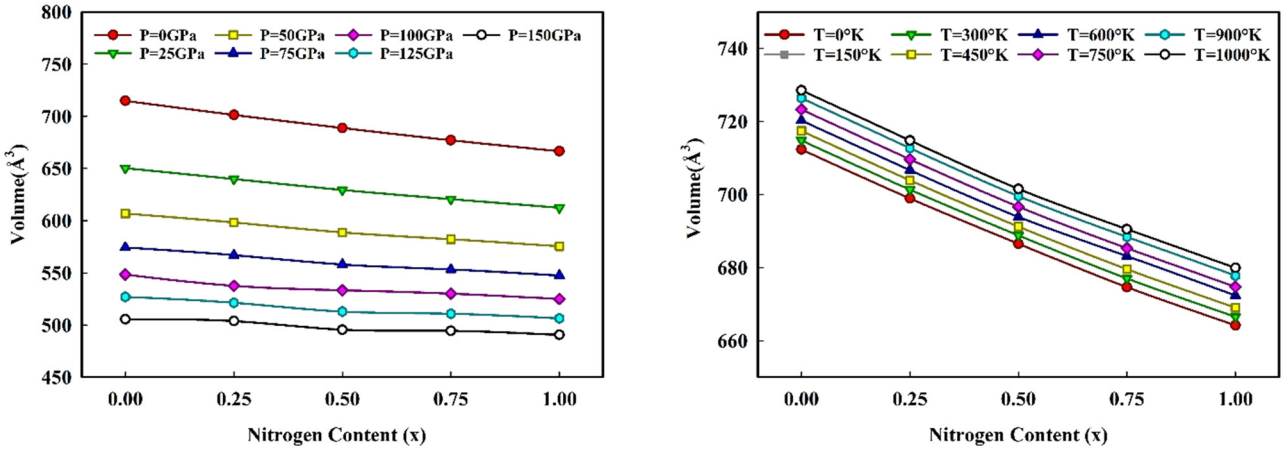

Figure 2: The volume of $ZrC_{(1-x)}N_x$ as a function of nitrogen content (x), (a) pressures, and (b) temperatures.

Table 2: Elastic constants (C_{ij}), elastic moduli (B, E, G), compressibility (ρ), and ductility/brittleness criteria for $ZrC_xN_{(1-x)}$

	Elastic constants (GPa)			Elastic moduli (GPa)			ρ (1/GPa)	Ductility/brittleness criterion		
	C_{11}	C_{12}	C_{44}	B	E	G		u	B/G	P_{Cauchy} (GPa)
ZrC	457	106	149	224	386	159	0.00628	0.211	1.401	−43
Expt.	472[a]	98[a]	159[a]	223[b]	390[b]	162[b]				
Others (GGA)	462[d]	102[d]	154[d]	220[c]	375[c]	155[c]				
Others (LDA)	499[e]	93[e]	170[e]	228[e]	435[e]	185[e]		0.18[e]		
$ZrC_{0.75}N_{0.25}$	503	99	158	232	419	174	0.00574	0.201	1.340	−59
Others				228[d]						
$ZrC_{0.50}N_{0.50}$	525	103	159	238	427	177	0.00565	0.206	1.371	−56
Others				235[c]	399[c]					
$ZrC_{0.25}N_{0.75}$	575	98	167	246	462	193	0.00519	0.200	1.335	−69
Others				241[d]						
ZrN	561	112	132	253	406	163	0.00612	0.241	1.603	−19
Expt.	471[g]	88[g]	138[g]	215[h]	390[c]	147[c]				
Others(GGA)	523[h]	107[h]	121[g]	246[f]	376[c]	135[c]				
Others(LDA)	548[i]	91[i]	117[i]	243[i]	434[i]	142[i]				
ZrAlC				125[j]	222[j]	92[j]		0.20[j]	0.74[j]	−24[j]

a. Ref. [79]; b. Ref. [59]; c. Ref. [28]; d. Ref. [50]; e. [80]; f. Ref. [76]; g. Ref. [81]; h. Ref. [77]; i. Ref. [78]; and j. Ref [82].

223 GPa, and the reported value in ref. [76], 220.6 GPa. For ZrN, the bulk modulus calculated from our simulations is 253.36 GPa, which has a fair agreement with 246.6 GPa, reported in ref. [76], and a considerable difference from the experimental value of 215 GPa. The highest Young's and shear moduli are obtained for $ZrC_{0.25}N_{0.75}$. The values of $\upsilon = 0.26$, $B/G = 1.75$, and $P_{Cauchy} = 0$ are the boundary values of the ductility and brittleness of the material. As seen, the structures are in the ductile region, and the ternary ceramics have higher brittleness than ZrC and ZrN; this is also true for the compressibility of structures. To compare the mechanical performance of the compound ceramics ($ZrC_{1-x}N_x$) with other Zr-based alloys, we bring in the elastic moduli of ZrAlC. As seen, the mechanical behavior of the $ZrC_{1-x}N_x$ is notably superior to that of the ZrAlC, which makes it more favorable for high-pressure applications like cutting tool materials.

Table 3 lists hardness, sound velocities, minimum thermal conductivity, melting temperature, and anisotropy indices for $ZrC_xN_{(1-x)}$. The hardness of the material is a measure of its resistance to plastic deformation. As expected (based on the values of ductility/brittleness criteria), the ternary compounds have a higher hardness. Also, due to the higher Young's modulus of ternary compounds, sound waves propagate faster in these compounds; this could be the reason for their higher thermal conductivity. The Debye temperature and melting point for the $ZrC_xN_{(1-x)}$ were calculated using the Anderson method [83] and Fine model [84–86], respectively. Based on this method, the $ZrC_{0.75}N_{0.25}$ has the highest Debye temperature and melting point among the structures. The anisotropy of structures increases, as the N-content increases, so that the ZrN features have the highest anisotropy.

3.2 Volume

Figure 2 presents the system's volume as a function of pressure and temperature (ZrC represents $x = 0$ and ZrN

Table 3: Hardness, sound velocities, minimum thermal conductivity, melting temperature, and anisotropy indices for $ZrC_xN_{(1-x)}$

	H_v (GPa)	v_t (m/s)	v_l (m/s)	v_m (m/s)	k_{min} (W/m.K)	T_{Debye} (K)	T_{melt} (K)	A_L	A_U
ZrC	23.18	4,939	8,167	5,459	1.660	689.1	3,253	0.0138	0.0309
$ZrC_{75}N_{25}$	26.05	5,103	8,344	5,634	1.748	715.8	3,524	0.0324	0.0724
$ZrC_{50}N_{50}$	25.57	5,083	8,359	5,616	1.757	718.1	3,657	0.0502	0.1135
$ZrC_{75}C_{25}$	27.95	5,269	8,606	5,817	1.843	747.9	3,950	0.0678	0.1539
ZrN	19.70	4,777	8,186	5,298	1.723	685.3	3,869	0.1494	0.3454

refers to $x = 1$). At higher pressures (at constant temperature), the volume decreases at a lower rate, signaling that the bulk modulus of structures increases by applying extra pressure. Similarly, as the nitrogen content increases, the structure shows more resistance to the volume change by adding to the applied pressure and temperature. For example, the volume change in ZrC ($x = 0$) and ZrN ($x = 1$) structures at 300 K, in a pressure range of 0–15 GPa, is 31.29 and 29.29%, respectively. Also, at zero pressure, with the temperature range of 0–1,000 K, ZrC, and ZrN show a volume change of 2.35 and 2.28%, respectively. This could be related to the lower compressibility, greater bulk modulus, and volume reduction of the structure in higher nitrogen content. Although the effect of applied pressure on the volume change might sound greater than the effect of thermal energy, since the temperature change and the applied pressure are of different orders, comparing the degree that volume has been affected by variation of each of these parameters might not be reasonable.

The resistance to the volume change could be related to the bonding strength of the structure, such that the structure with shorter interatomic bonds shows higher resistance to the volume change. On the other hand, as stated earlier, the bulk modulus is a measure of the structure's resistance to volume change. Hence, the structure with shorter bonds is expected to have a higher bulk modulus. N atoms have a smaller radius than C atoms; therefore, the Zr–N bond is stronger than the Zr–C bond. This could explain the higher bulk modulus of ZrN compared to ZrC. Applying the same analogy might help describe the behavior of the $ZrC_{(1-x)}N_x$ compounds. By increasing x, the contribution of Zr–N bonds becomes stronger, which could explain the increasing bulk modulus with x. In Figure 3, the isothermal bulk modulus in different pressures (a) and temperatures (b) has been presented as a function of nitrogen content. In Figure 3a, the temperature has been fixed at 300 K. As seen, in all structures, the isothermal bulk modulus increases with increasing pressure. This could be ascribed to the contraction of bonds, greater repulsion of atoms, and hence stronger bonding in the crystal. At 150 GPa, the isothermal bulk modulus of ZrC and ZrN has been increased by 234.17 and 256.04%, respectively. In Figure 3b, the applied pressure equals to the ambient pressure. With increasing the temperature to 150 K, the isothermal bulk modulus slightly decreases, but a higher reduction is observed for higher temperatures. In lower temperatures, the magnitude of the phonon vibrations is not high enough to increase the length of the bonds and hence weaken their strength. However, in the temperature range of >150 K, due to the induced thermal stress, phonon vibrations become intense enough that smaller temperature increment could affect (increase) the bond length and their softening rate. Increasing the temperature up to 1,000 K results in a 9.69 and 12.42% decrease in the isothermal bulk modulus of ZrC and ZrN, respectively. As seen in Figure 3, the bulk modulus increases by increasing the nitrogen content. The $ZrC_{0.50}N_{0.50}$ structure has been influenced differently than the other compounds, as it shows a lower increase in pressure (Figure 3a) and a smaller decrease in temperature (Figure 3b). The coexistence of different types of interatomic forces, resembles a mechanical stress and leads to the structural anisotropy of the system. This anisotropy has its highest value in the $ZrC_{0.50}N_{0.50}$ structure.

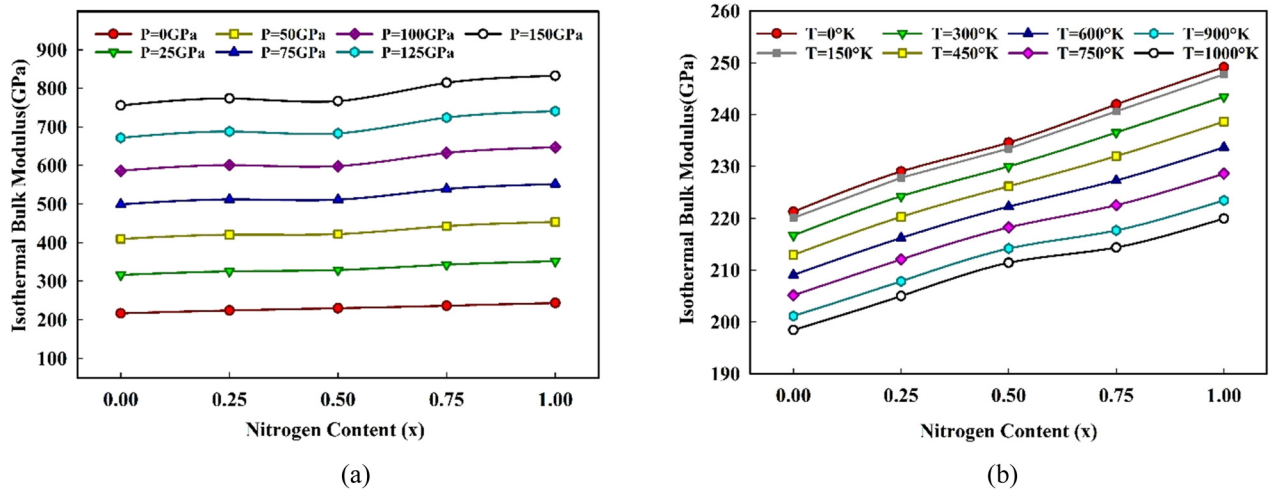

(a) (b)

Figure 3: Isothermal bulk modulus of $ZrC_{(1-x)}N_x$ as a function of nitrogen content (x) for (a) different pressures at 300 K and (b) different temperatures at zero pressure.

3.3 Entropy

We calculated the entropy of $ZrC_{(1-x)}N_x$ against temperature, pressure, and nitrogen content (x), as shown in Figure 4. Each parameter impacts the entropy through its associated mechanism; temperature via affecting the interatomic force constants, pressure through volume change, and nitrogen content by the difference in atomic size and mass, electronegativity, electron-to-atom ratio, effective mass, or band filling phenomenon in Zr–C and Zr–N bonds. As seen in Figure 4a, by increasing the pressure (at 300 K), the entropy drops in all structures, which is attributed to the reduction of system volume and the enhancement of the resistance of bonds to the length change. Reduction of volume diminishes the degree of disorder, or the phonon vibrations take place with limited amplitude. In other words, increasing the pressure limits/decreasing the frequency of vibrations is equivalent to driving the system toward a higher order level. The effect of increasing temperature on entropy is shown in Figure 4b. Temperature increase results in volume expansion, bond softening, and the atoms' excitement toward vibration with higher frequency. With the expansion of volume, the disorder's degree also increases. Similarly, increasing the energy increases the density of interactions. Softening also leads to a higher frequency of vibrations. As mentioned earlier, increasing the nitrogen content could have a multifaceted effect on the entropy, possibly counterbalancing each other. Replacing the C atoms with N atoms increases the number of electrons in the system, which could be interpreted as higher entropy. However, ZrN bonds added to the system (as x increases) have a shorter length than the pre-existing ZrC bonds. So, phonon vibrations decline, and the entropy decreases. Two competing effects of N atoms on the entropy were introduced; however, taking Figure 4 into account, we conclude that the electronegativity and reduction of bonding length is the dominant effect, and the entropy of $ZrC_{(1-x)}N_x$ structures decrease with x [31]. Nevertheless, there exists an exclusion at $x = 0.5$, becoming more noticeable at higher pressures. This compound has the lowest entropy drop among the other compounds, which has appeared as a peak in the plot. Table 4 contains the Gibbs free energy and the contribution of phonon vibrations in free Helmholtz energy of structures at the pressures of 0 and 150 GPa. The pressure-induced increase in anisotropy has affected the reducing rate of the Gibbs energy in the $ZrC_{0.50}N_{0.50}$ structure, signaling lower stability of this compound compared to the others. Moreover, the amount of reduction in vibration-induced energy due to applying a pressure of 150 GPa is the lowest for $ZrC_{0.50}N_{0.50}$. It is also worth noting that the influence of the pressure change on the entropy is significantly lower than the temperature change.

3.4 Grüneisen

Figure 5 presents a variation of the Grüneisen parameter by temperature, pressure, and nitrogen content (x) for $ZrC_{(1-x)}N_x$ structures. This parameter describes the effect of volume change on the vibrations and dynamics of the crystal lattice. A change in temperature, pressure, or content of constituent atoms could cause this volume change.

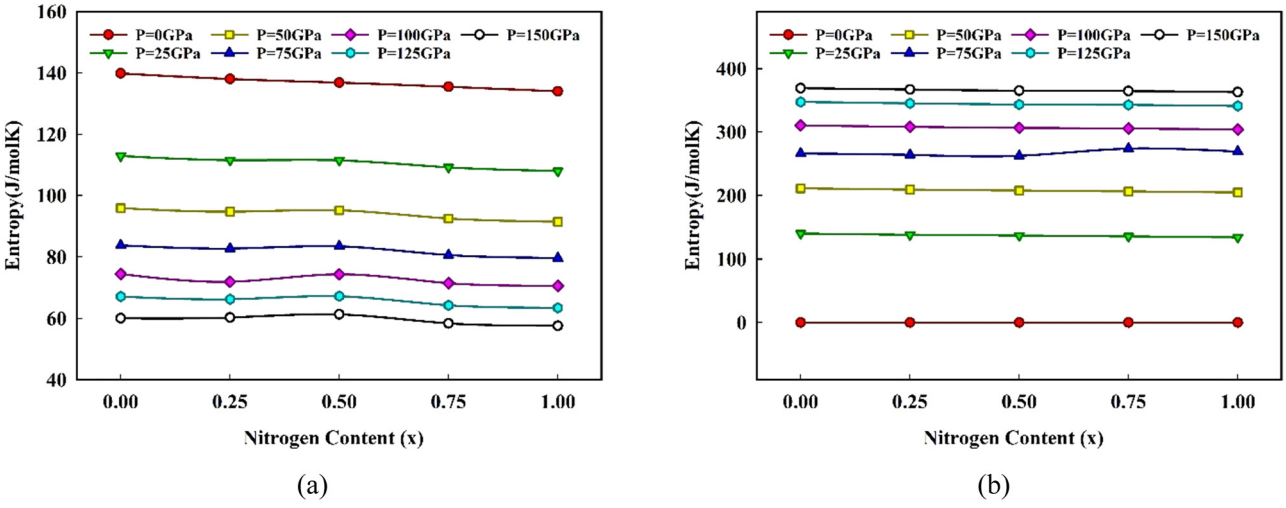

Figure 4: Entropy of $ZrC_{(1-x)}N_x$ as a function of nitrogen content (x) for (a) different pressures at 300 K and (b) different temperatures at zero pressures.

Table 4: Gibbs free energy values and the contribution of the vibration in *G* at the pressure of 150 GPa

	P (GPa)	ZrC	$ZrC_{0.75}N_{0.25}$	$ZrC_{0.50}C_{0.50}$	$ZrC_{0.25}N_{0.75}$	ZrN
G (kJ·mol^{-1})	0	−9,549,936	−9,560,920	−9,571,897	−9,582,869	−9,593,835
	150	−9,547,977	−9,558,987	−9,569,995	−9,580,985	−9,591,972
Δ*G* (kJ·mol^{-1})		1959.334	1932.938	1901.551	1883.922	1863.147
F_{vib} (kJ·mol^{-1})	0	7.565	7.772	7.905	8.059	8.229
	150	19.165	19.347	19.119	19.766	19.944
ΔF_{vib} (kJ·mol^{-1})		11.601	11.575	11.214	11.707	11.714

The dependency of Grüneisen on the volume change could be explained from two aspects. First, by the change in the compressibility of the structure, and second, by altering the phonon vibrations (i.e., entropy). As shown in Figure 5a, by increasing pressure, Grüneisen continuously decreases. Given the discussion about the variation of the volume and entropy by pressure, it could be stated that volume drop dominates the entropy drop by pressure increase. Therefore, Grüneisen drops constantly by pressure, and equation (9) confirms this trend. Moreover, as the applied pressure increases, the rate at which the Grüneisen declines also decreases, which could be related to the reduction of compressibility of the crystal by pressure. In Figure 3b, in which the variation of the Grüneisen parameter with temperature has been presented, the opposite profile is observed; Grüneisen increases with temperature. Temperature increase leads to volume expansion, bond softening, and an increase in entropy. The rate of the changes also grows with the temperature, which is due to the lower resistance of the lattice to the volume change and the higher extent of disorder in the system. Nitrogen content affects both the volume change and the entropy. Still, the behavior of the $ZrC_{0.50}N_{0.50}$ structure differs from the others as it has the lowest Grüneisen parameter in Figure 3. The nitrogen content (*x*) is directly related to the Grüneisen; however, this observation is not justified with the obtained results.

3.5 Thermal expansion

Any change in the lattice condition, e.g., applying pressure, changing temperature, or content of the elements, could affect bond characterizations, such as length, strength, and the vibrational response of the atoms in the bonds. Figure 6 presents the effect of temperature, pressure, and nitrogen content on thermal expansion. As seen in Figure 6a, pressure increase has a similar, reducing effect on the thermal expansion. The temperature increase, however, in all structures results in an enhancement of the thermal expansion coefficient. The effect of pressure comes from the reduction of compressibility and the entropy of the structure. Conversely, the effect of temperature originates from the structure's softening and increasing entropy. In lower pressures and temperatures, thermal expansion has been affected considerably higher. Literature has reported

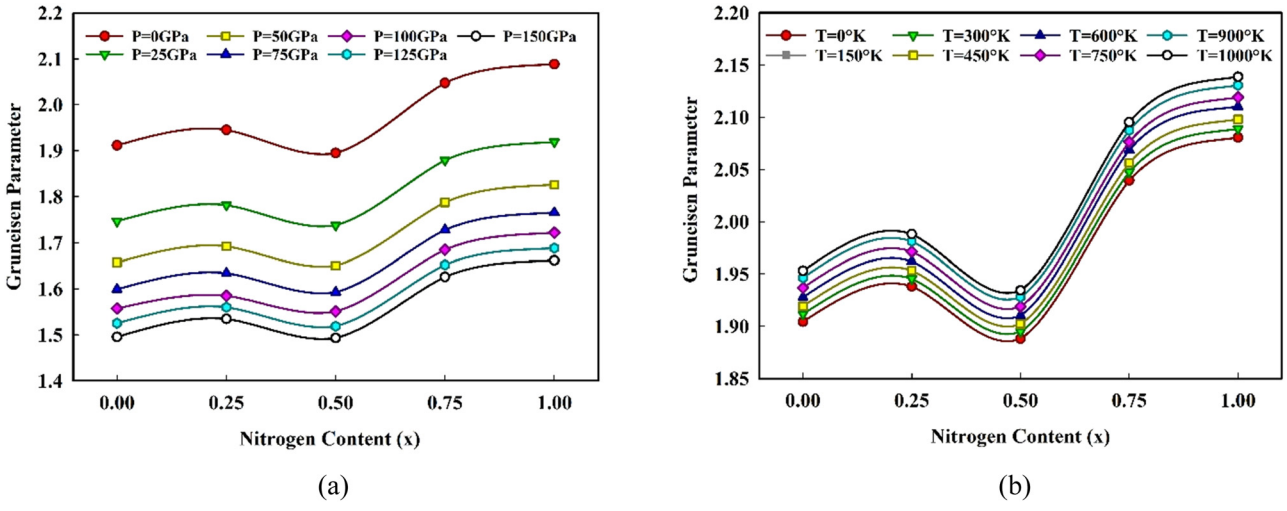

Figure 5: Grüneisen of $ZrC_{(1-x)}N_x$ as a function of nitrogen content (*x*) for (a) different pressures at 300 K and (b) different temperatures at zero pressures.

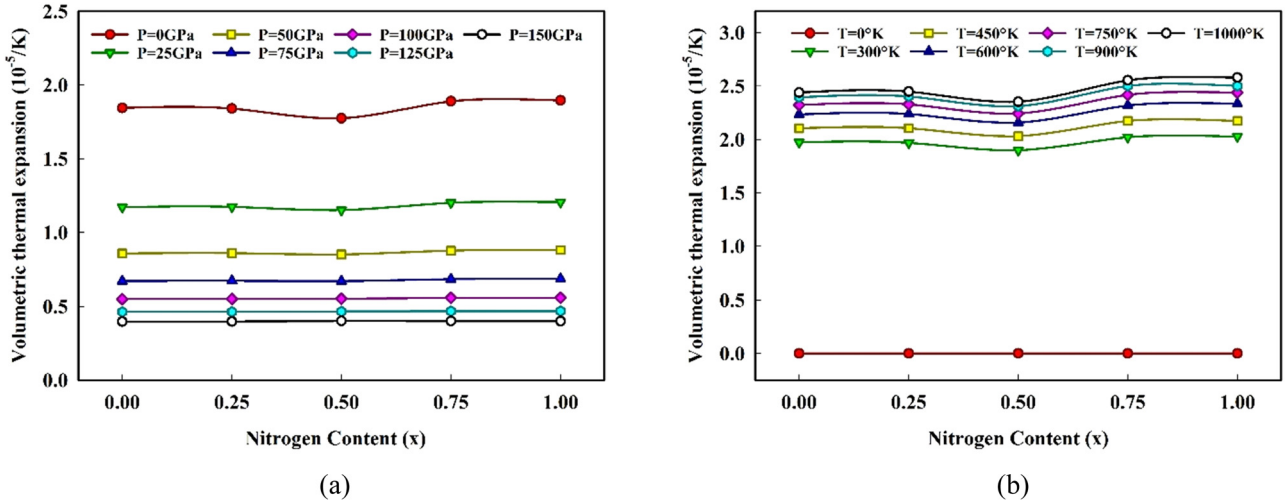

Figure 6: Volumetric expansion coefficient of $ZrC_{(1-x)}N_x$ as a function of nitrogen content (x) for (a) different pressures at 300 K and (b) different temperatures at zero pressure.

a T^3 correlation in the intermediate temperature range and a linear relation at higher temperatures [63]. Another affecting parameter on the volumetric expansion coefficient is the nitrogen content. As seen, the nitrogen content has a negligible effect on the thermal expansion at high pressures and low temperatures.

3.6 Heat capacity

Since the heat capacity mostly depends on the long-wave lattice vibrations, variation of the heat capacity due to external factors (e.g., temperature and pressure) and compositional changes could be related to the alternation in the number of excited phonon modes [31,59]. We report the analysis of C_v and C_p in Figures 7 and 8. The difference between the two parameters arises from the anharmonic effects of thermal expansion, which could be inferred from equations (11) and (12) [31,59]. Increasing the pressure at a temperature of 300 K causes the C_v to decrease, where the reduction rate drops with pressure. A similar trend is visible for the C_p at different temperatures. It should be noted that at higher temperatures, the effect of the pressure becomes weaker, which could be ascribed to the suppression of anharmonic effects on the heat capacity [63,87]; in other words, dependency on the

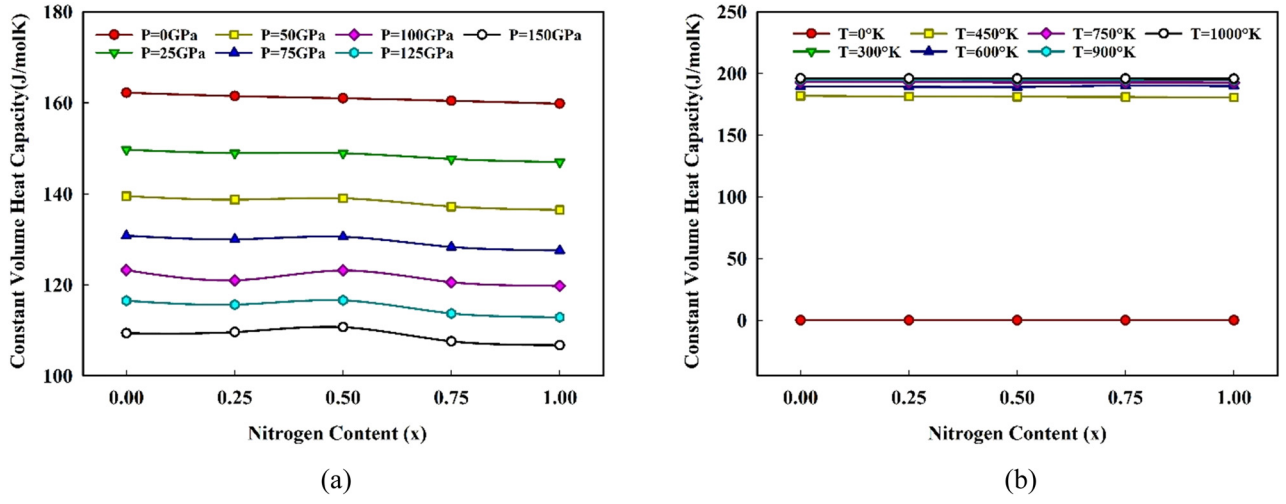

Figure 7: Constant volume specific heat of $ZrC_{(1-x)}N_x$ as a function of nitrogen content (x) for (a) different pressures at 300 K and (b) different temperatures at zero pressures.

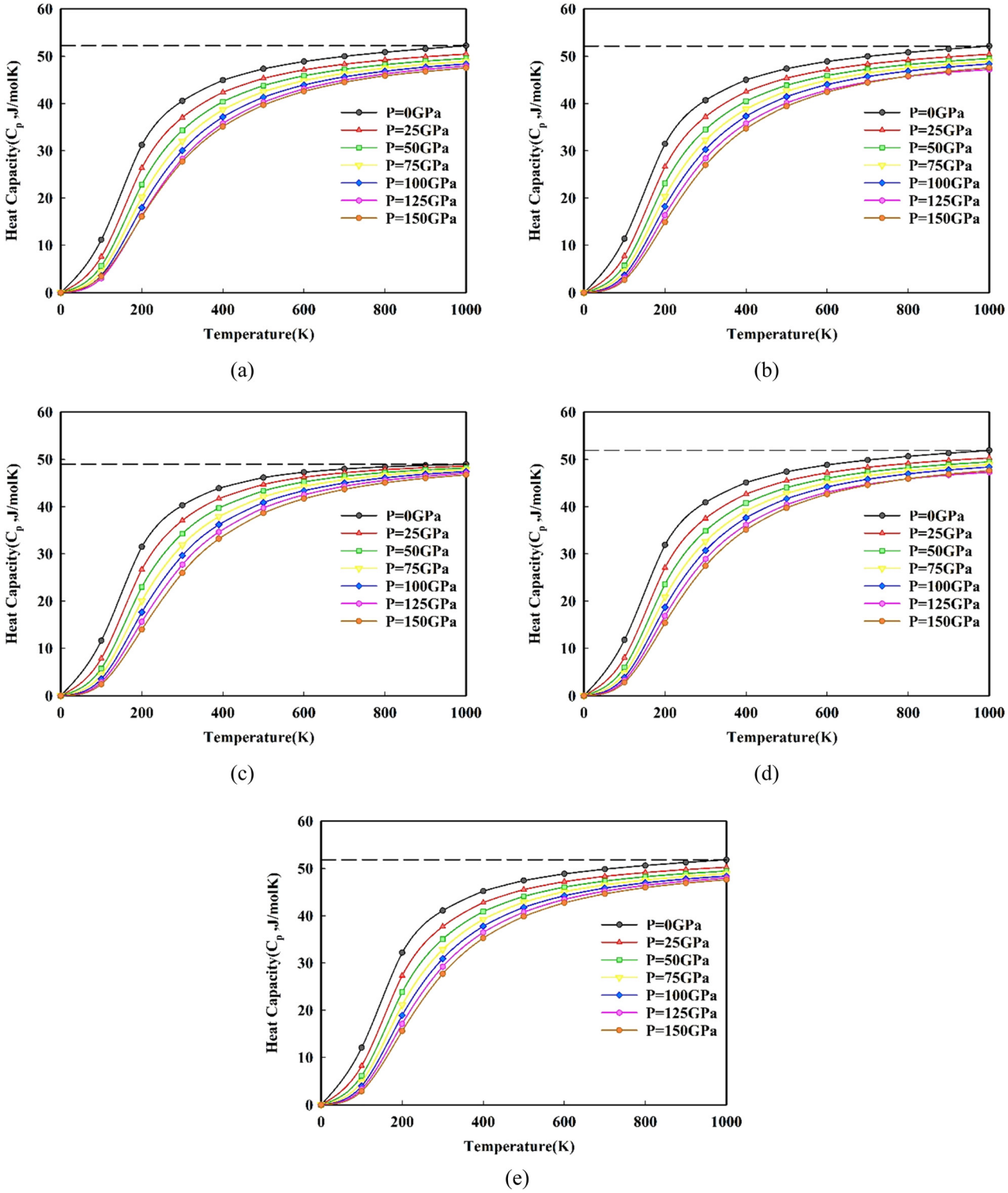

Figure 8: Constant pressure heat capacity as a function of temperature and for different pressures for (a) ZrC, (b) $ZrC_{0.75}N_{0.25}$, (c) $ZrC_{0.50}N_{0.50}$, (d) $ZrC_{0.25}N_{0.75}$, and (e) ZrN.

temperature and pressure becomes weaker. The temperature has a higher impact on the heat capacity than the pressure. Increasing temperature increases heat capacity, which originates from phonon thermal softening [68]. The extent of the influence is a function of temperature, for which some descriptive models have been developed.

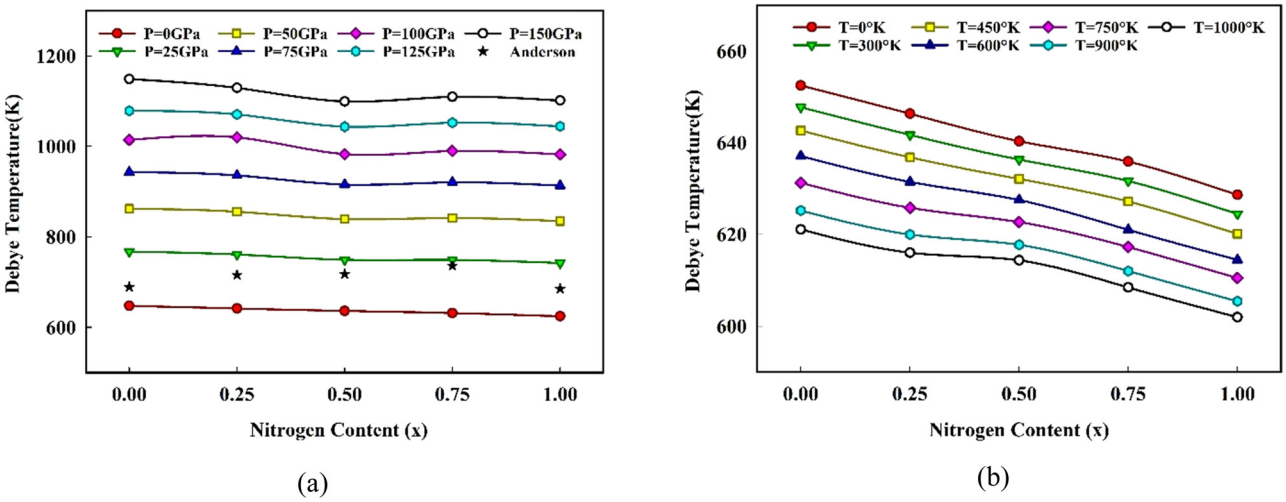

Figure 9: Debye temperature for structures of $ZrC_{(1-x)}N_x$ as a function of nitrogen content (x) for (a) different pressures at 300 K and (b) different temperatures at zero pressure.

The Debye model is one of these models that is valid in the low-temperature range. Generally, the temperature-dependent behavior of the heat capacity at low and high temperatures has quantum and classical aspects, respectively [27,88]. In the quantum approach, the low-temperature behavior of the heat capacity is affected by the density of states of the acoustic phonons at low phonon frequencies. In this temperature range, heat capacity has a T^3 correlation with the temperature due to the long-wavelength acoustic phonons [27,89]. By increasing the temperature toward the Debye temperature, the classic behavior takes over. The classic model resembles Einstein's model in which heat capacity is exponentially related to the temperature. Finally, heat capacity reaches a constant value called the Dulong–Petit limit in all structures at temperatures far above the Debye temperature. This indicates that the supplied thermal energy has excited all phonon modes, leading to saturation of vibrational bonds [8,27,90,91]. In Figure 7b, it is shown that at 0 K, C_v amounts to zero. By increasing the temperature, C_v increases with a T^3 profile (the Debye model) up to 200 K. After reaching the Debye temperature, it follows an exponential profile and finally approaches the Dulong–Petit constant value. The temperature-wise behavior of C_p is shown in Figure 8. In all structures, C_p shows an increasing trend with the temperature (as with C_v), but when a pressure increase accompanies it, the increasing rate becomes smaller. Another point to be mentioned is that the heat capacity increases by adding N atoms to the ZrC structure. Furthermore, for $ZrC_{0.50}N_{0.50}$, the reduction of heat capacity by pressure is lower.

3.7 Debye temperature

Given 0 K as the onset point with no vibrational mode, the vibration of atoms increases by temperature. Debye temperature is a temperature at which the atomic vibrational modes are maximum in magnitude [92]. Temperature, pressure, and material composition are among the parameters that affect the Debye temperature. Figure 9 presents the Debye temperature of $ZrC_{(1-x)}N_x$ structures as a function of pressure (a) and temperature (b). As seen in Figure 9a, Debye temperature continuously increases with pressure, which is mostly because of the reduction of lattice constant. By reducing the lattice constant, the maximum frequency of thermal vibrations and corresponding equivalent temperature increases [54]. The values of T_{Debye} for the compounds calculated via the Anderson method are also depicted in Figure 9a, agreeing with the values obtained from Debye–Grüneisen quasi-harmonic model. In Figure 9b, on the contrary, in all structures, the Debye temperature decreases with temperature. This stems from the volume expansion and increase of the interatomic distances, which weaken the bonding of atoms. As previously mentioned, since Zr–N bonds are shorter than Zr–C bonds, the volume of the structure becomes continuously smaller by adding the N atoms to the ZrC crystal. So, as seen in Figure 9a and b, the Debye temperature decreases by nitrogen content. The reduction, however, is lower in the $ZrC_{0.50}N_{0.50}$ structure, such that it has the lowest value at high pressures. The same is valid with the temperature increase, as this structure has the lowest step-wise drop and, accordingly, highest Debye

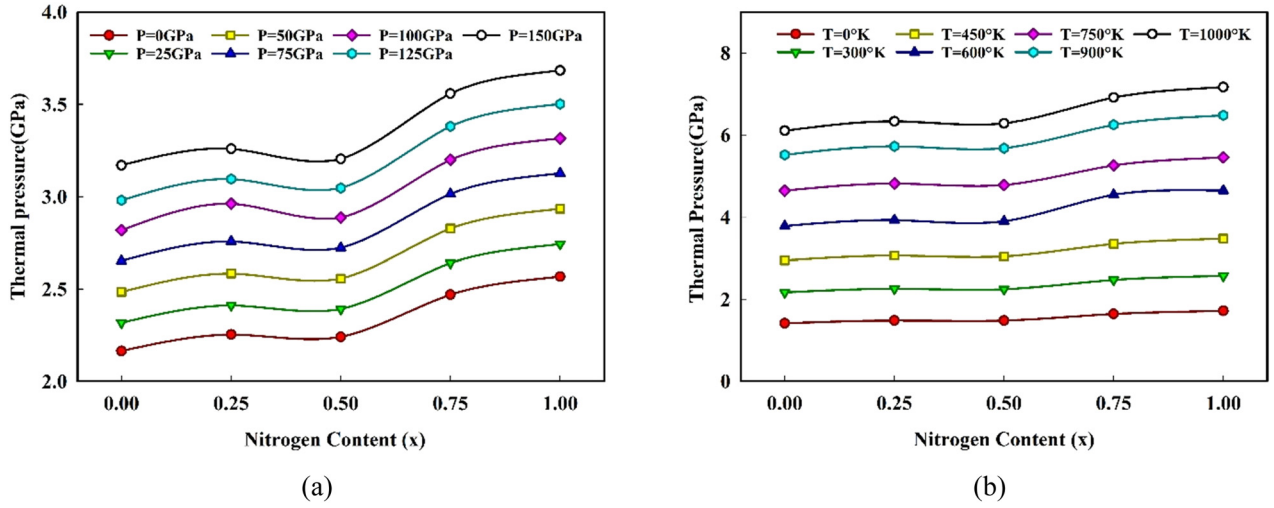

Figure 10: Thermal pressure of $ZrC_{(1-x)}N_x$ as a function of nitrogen content (x) for (a) different pressures at 300 K and (b) different temperatures at zero pressures.

temperature (compared to the other ternary compounds) in the high-temperature range. Debye temperature has a different behavior from the isothermal bulk modulus. The Debye temperature of the $ZrC_{0.50}N_{0.50}$ structure is less affected upon increasing pressure and temperature.

3.8 Thermal pressure

Figure 10 shows the variation of thermal pressure of $ZrC_{(1-x)}N_x$ structures as a function of pressure and temperature. In Figure 10a, the temperature is fixed at 300 K, and the values in Figure 10b were obtained at zero pressure. Thermal pressure increases with temperature. Thermal pressure is a component of total pressure representing the effect of phonon vibrations caused by temperature increase. At ambient pressure conditions, this part is canceled out by the negative static pressure so that the net applied pressure becomes zero. By increasing the temperature, phonon energy is at a higher level, resulting in higher thermal pressure. Overall, the dependency of thermal pressure on temperature is stronger than the pressure. As seen in Figure 10a, it has been slightly affected by pressure increase. Taking the $ZrC_{0.50}N_{0.50}$ structure as an exclusion, nitrogen content has an increasing effect on thermal pressure in different temperatures and pressures (in the low-pressure range, the rate is lower). $ZrC_{0.50}N_{0.50}$ structure has the lowest thermal pressure among all ternary compounds in all pressures and temperatures.

4 Conclusion

We performed DFT calculations to investigate the thermal properties of $ZrC_{(1-x)}N_x$ ceramics at extreme conditions, with x being 0.0, 0.25, 0.5, 0.75, 1.0. The temperature varied from 0 to 1,000 K, and the pressure range was chosen to be 0–150 GPa. In our investigation, we covered elastic constants, elastic moduli, compressibility, ductility/brittleness, hardness, sound velocities, minimum thermal conductivity, melting temperature, anisotropy indices, isothermal bulk modulus, heat capacities, entropy, Debye temperature, Grüneisen parameter, thermal expansion coefficient, and thermal pressure. We used the Debye–Grüneisen quasi-harmonic model to account for temperature and pressure effects. We consider the anisotropy and the bonding nature of the structure in analyzing the compounds' behavior. Pressure has a direct effect on the bulk modulus and thermal pressure and inversely affects the heat capacity and thermal expansion. Predictably, temperature affects these properties oppositely. However, the extent to which each property is affected by temperature and pressure increase, is different. $ZrC_{0.50}N_{0.50}$ shows a similar qualitative but different quantitative response in all properties, such that the effect of applied conditions is different with respect to the other compounds. Considering the thermal expansion and heat capacity, we conclude that $ZrC_{0.50}N_{0.50}$ could perform better than the other compounds in high temperature and pressure conditions. This feature could make the $ZrC_{0.50}N_{0.50}$ ternary compound more favorable over

frequently used ZrC and ZrN binaries in industrial coating applications. The increase of thermal expansion at elevated temperature negatively impacts the adhesion of the coating material to the target substrate. Moreover, a smaller variation of heat capacity by pressure at high temperatures is desired in confronting off-design conditions; namely the operational efficiency of the coatings of the gas turbine blades.

Acknowledgment: The support from Shahid Beheshti University is gratefully acknowledged.

Funding information: The authors state no funding involved.

Author contributions: Hassan Alipour performed the simulations, analyzed the results, and wrote the main manuscript text. Ali. Hamedani has a contribution in analyzing the results and writing the main manuscript text. Ghasem Alahyarizadeh supervised and conducted the whole work and the manuscript. All authors reviewed the manuscript.

Conflict of interest: The authors state no conflict of interest.

Data availability statement: Data sharing is not applicable to this article as no datasets were generated or analyzed during the current study.

Code availability: There was not any code data related to the research.

References

[1] Oyama, S. T. Introduction to the chemistry of transition metal carbides and nitrides. In: *Chem. Transit. Met. Carbides Nitrides*, Springer, Dordrecht, 1996, pp. 1–27.

[2] Xiao, Y., J.-Y. Hwang, and Y.-K. Sun. Transition metal carbide-based materials: synthesis and applications in electrochemical energy storage. *Journal of Materials Chemistry A: Materials for Energy and Sustainability*, Vol. 4, 2016, pp. 10379–10393.

[3] Katoh, Y., G. Vasudevamurthy, T. Nozawa, and L. L. Snead. Properties of zirconium carbide for nuclear fuel applications. *Journal of Nuclear Materials*, Vol. 441, 2013, pp. 718–742.

[4] Maibam, J. Investigation of electronic band structure of transition metal carbides and nitrides using density functional theory, PhD Thesis, Assam University, 2013.

[5] Saha, B., J. Acharya, T. D. Sands, and U. V. Waghmare. Electronic structure, phonons, and thermal properties of ScN, ZrN, and HfN: A first-principles study. *Journal of Applied Physics*, Vol. 107, 2010, id. 33715.

[6] Zhu, J., B. Zhu, J. Qu, Q. Gou, and F. Chen. Thermodynamic properties of cubic ZrC under high pressure from first-principles calculations. *Science in China Series G: Physics, Mechanics and Astronomy*, Vol. 52, 2009, pp. 1039–1042.

[7] Alipour, H., A. Hamedani, G. Alahyarizadeh, and A. Jahanzadeh. First principle study on the mechanical response of ZrC and ZrN at high-pressure conditions: anisotropy perspective. *Molecular Simulation*, Vol. 47, 2021, pp. 1135–1148.

[8] Harrison, R. W. and W. E. Lee. Processing and properties of ZrC, ZrN and ZrCN ceramics: a review. *Advances in Applied Ceramics*, Vol. 115, 2016, pp. 294–307.

[9] Souadia, Z., A. Bouhemadou, R. Khenata, and Y. Al-Douri. Structural, elastic and lattice dynamical properties of the alkali metal tellurides: First-principles study. *Physica B: Condensed Matter*, Vol. 521, 2017, pp. 204–214.

[10] Bidai, K., M. Ameri, S. Amel, I. Ameri, Y. Al-Douri, D. Varshney, et al. First-principles calculations of pressure and temperature dependence of thermodynamic properties of anti-perovskite $BiNBa_3$ compound. *Chinese Journal of Physics*, Vol. 55, 2017, pp. 2144–2155.

[11] Otero-de-la-Roza, A., D. Abbasi-Pérez, and V. Luaña. Gibbs2: A new version of the quasiharmonic model code. II. Models for solid-state thermodynamics, features and implementation. *Computer Physics Communications*, Vol. 182, 2011, pp. 2232–2248.

[12] Benkabou, M. H., M. Harmel, A. Haddou, A. Yakoubi, N. Baki, R. Ahmed, et al. Structural, electronic, optical and thermodynamic investigations of $NaXF_3$ (X = Ca and Sr): First-principles calculations. *Chinese Journal of Physics*, Vol. 56, 2018, pp. 131–144.

[13] Hadji, S., A. Bouhemadou, K. Haddadi, D. Cherrad, R. Khenata, S. Bin-Omran, et al. Elastic, electronic, optical and thermodynamic properties of $Ba_3Ca_2Si_2N_6$ semiconductor: First-principles predictions. *Physica B: Condensed Matter*, Vol. 589, 2020, id. 412213.

[14] Ayad, M., F. Belkharroubi, F. Z. Boufadi, M. Khorsi, M. K. Zoubir, M. Ameri, et al. First-principles calculations to investigate magnetic and thermodynamic properties of new multifunctional full-Heusler alloy Co_2TaGa. *Indian Journal of Physics and Proceedings of the Indian Association for the Cultivation of Science*, Vol. 94, 2020, pp. 767–777.

[15] Mentefa, A., F. Z. Boufadi, M. Ameri, F. Gaid, L. Bellagoun, A. A. Odeh, et al. First-principles calculations to investigate structural, electronic, elastic, magnetic, and thermodynamic properties of full-Heusler Rh_2MnZ (Z = Zr, Hf). *Journal of Superconductivity and Novel Magnetism*, Vol. 34, 2021, pp. 269–283.

[16] Cao, C. L., Z. F. Hou, and G. Yuan. First-principles study of the structural stability and electronic structures of TaN. *Physica Status Solidi*, Vol. 245, 2008, pp. 1580–1585.

[17] Koelling, D. D. and G. O. Arbman. Use of energy derivative of the radial solution in an augmented plane wave method: application to copper. *Journal of Physics F: Metal Physics*, Vol. 5, 1975, id. 2041.

[18] Al-Douri, Y., M. Ameri, A. Bouhemadou, and K. M. Batoo. First-principles calculations to investigate the refractive index and optical dielectric constant of Na_3SbX_4 (X = S, Se) ternary chalcogenides. *Physica Status Solidi*, Vol. 256, 2019, id. 1900131.

[19] Jepsen, O., M. Snob, and O. K. Andersen. Linearized band structure methods in electronic band-structure and its applications. *Springer Lect. Notes*, Springer, Berlin, 1987.
[20] Zoubir, M. K., B. Fadila, B. Keltoum, A. Ibrahim, B. L. Farah, Y. Al-Douri, et al. Structural, electronic and thermodynamic investigation of Ag_2GdSi, Ag_2GdSn and Ag_2Gd Pb Heusler alloys: First-principles calculations. *Materials Testing*, Vol. 63, 2021, pp. 537–542.
[21] Ameri, M., F. Bennar, S. Amel, I. Ameri, Y. Al-Douri, and D. Varshney. Structural, elastic, thermodynamic and electronic properties of LuX (X = N, Bi and Sb) compounds: first principles calculations. *Phase Transitions*, Vol. 89, 2016, pp. 1236–1252.
[22] Parr, R. G. Density functional theory of atoms and molecules. In: *Horizons Quantum Chem*, Springer, Dordrecht, 1980, pp. 5–15.
[23] Perdew, J. P., J. A. Chevary, S. H. Vosko, K. A. Jackson, M. R. Pederson, D. J. Singh, et al. Atoms, molecules, solids, and surfaces: Applications of the generalized gradient approximation for exchange and correlation. *Physical Review B*, Vol. 46, 1992, id. 6671.
[24] Perdew, J. P., K. Burke, and M. Ernzerhof. Generalized gradient approximation made simple. *Physical Review Letters*, Vol. 77, 1996, id. 3865.
[25] Asma, B., F. Belkharroubi, A. Ibrahim, B. Lamia, A. Mohammed, W. Belkilali, et al. Structural, mechanical, magnetic, electronic, and thermal investigations of Ag_2YB (Y = Nd, Sm, Gd) full-Heusler alloys. *Emergent Mater*, Vol. 4, 2021, pp. 1769–1783.
[26] Zhao, E., J. Wang, J. Meng, and Z. Wu. Structural, mechanical and electronic properties of 4d transition metal mononitrides by first-principles. *Computational Materials Science*, Vol. 47, 2010, pp. 1064–1071.
[27] Hao, A., T. Zhou, Y. Zhu, X. Zhang, and R. Liu. First-principles investigations on electronic, elastic and thermodynamic properties of ZrC and ZrN under high pressure. *Materials Chemistry and Physics*, Vol. 129, 2011, pp. 99–104.
[28] Kim, J. and Y. J. Suh. Temperature-and pressure-dependent elastic properties, thermal expansion ratios, and minimum thermal conductivities of ZrC, ZrN, and Zr ($C_{0.5}N_{0.5}$). *Ceramics International*, Vol. 43, 2017, pp. 12968–12974.
[29] Jing, Q., C. Wu, and H. Gong. Phase transition, thermodynamic and elastic properties of ZrC. *Transactions of Nonferrous Metals Society of China*, Vol. 28, 2018, pp. 2520–2527.
[30] Varshney, D. and S. Shriya. Elastic, mechanical and thermodynamic properties at high pressures and temperatures of transition metal monocarbides. *International Journal of Refractory Metals and Hard Materials*, Vol. 41, 2013, pp. 375–401.
[31] Yang, Y., L. Ma, G.-Y. Gan, W. Wang, and B.-Y. Tang. Investigation of thermodynamic properties of high entropy (TaNbHfTiZr) C and (TaNbHfTiZr) N. *Journal of Alloys and Compounds*, Vol. 788, 2019, pp. 1076–1083.
[32] Radja, K., B. L. Farah, A. Ibrahim, D. Lamia, I. Fatima, B. Nabil, et al. Investigation of structural, magneto-electronic, elastic, mechanical and thermoelectric properties of novel lead-free halide double perovskite Cs_2AgFeC_{l6}: First-principles calculations. *Journal of Physics and Chemistry of Solids*, Vol. 167, 2022, id. 110795.
[33] Khireddine, A., A. Bouhemadou, S. Maabed, S. Bin-Omran, R. Khenata, and Y. Al-Douri. Elastic, electronic, optical and thermoelectric properties of the novel Zintl-phase Ba_2ZnP_2. *Solid State Sciences*, Vol. 128, 2022, id. 106893.
[34] Hasni, L., M. Ameri, D. Bensaid, I. Ameri, S. Mesbah, Y. Al-Douri, et al. First-principles calculations of structural, magnetic electronic and optical properties of rare-earth metals TbX (X = N, O, S, Se). *Journal of Superconductivity and Novel Magnetism*, Vol. 30, 2017, pp. 3471–3479.
[35] Boudiaf, K., A. Bouhemadou, O. Boudrifa, K. Haddadi, F. S. Saoud, R. Khenata, et al. Structural, elastic, electronic and optical properties of LaOAgS-type silver fluoride chalcogenides: First-principles study. *Journal of Electronic Materials*, Vol. 46, 2017, pp. 4539–4556.
[36] Belkilali, W., F. Belkharroubi, M. Ameri, N. Ramdani, F. Boudahri, F. Khelfaoui, et al. Theoretical investigations of structural, mechanical, electronic and optical properties of NaScSi alloy. *Emergent Mater*, Vol. 4, 2021, pp. 1465–1477.
[37] Fadila, B., M. Ameri, D. Bensaid, M. Noureddine, I. Ameri, S. Mesbah, et al. Structural, magnetic, electronic and mechanical properties of full-Heusler alloys Co_2YAl (Y = Fe, Ti): First principles calculations with different exchange-correlation potentials. *Journal of Magnetism and Magnetic Materials*, Vol. 448, 2018, pp. 208–220.
[38] Khireddine, A., A. Bouhemadou, S. Alnujaim, N. Guechi, S. Bin-Omran, Y. Al-Douri, et al. First-principles predictions of the structural, electronic, optical and elastic properties of the Zintl-phases AE_3GaAs_3 (AE = Sr, Ba). *Solid State Sciences*, Vol. 114, 2021, id. 106563.
[39] Guechi, N., A. Bouhemadou, Y. Medkour, Y. Al-Douri, R. Khenata, and S. Bin-Omran. Electronic and thermoelectric properties of the layered Zintl phase $CaIn_2P_2$: first-principles calculations. *Philosophical Magazine*, Vol. 100, 2020, pp. 3023–3039.
[40] Boudiaf, K., A. Bouhemadou, Y. Al-Douri, R. Khenata, S. Bin-Omran, and N. Guechi. Electronic and thermoelectric properties of the layered BaFAgCh (Ch = S, Se and Te): First-principles study. *Journal of Alloys and Compounds*, Vol. 759, 2018, pp. 32–43.
[41] Benkaddour, Y., A. Abdelaoui, A. Yakoubi, H. Khachai, Y. Al-Douri, S. Bin Omran, et al. First-principle calculations of structural, elastic, and electronic properties of intermetallic rare earth R_2Ni_2Pb (R = Ho, Lu, and Sm) compounds. *Journal of Superconductivity and Novel Magnetism*, Vol. 31, 2018, pp. 395–403.
[42] Yahiaoui, I. E., A. Lazreg, Z. Dridi, Y. Al-douri, and B. Bouhafs. Gd impurities effect on Co_2CrSi alloy: first-principle calculations. *Bulletin of Materials Science*, Vol. 41, 2018, id. 1.
[43] Touam, S., R. Belghit, R. Mahdjoubi, Y. Megdoud, H. Meradji, M. S. Khan, et al. First-principles computations of $Y_xGa_{1-x}As$-ternary alloys: a study on structural, electronic, optical and elastic properties. *Bulletin of Materials Science*, Vol. 43, 2019, id. 22.
[44] Blaha, P., K. Schwarz, G. K.H. Madsen, D. Kvasnicka, J. Luitz, R. Laskowsk, et al. An augmented plane wave + local orbitals program for calculating crystal properties. *Techn, Univ*, Wien, Austria, 2001.
[45] Schwarz, K. and P. Blaha. Solid state calculations using WIEN2k. *Computational Materials Science*, Vol. 28, 2003, pp. 259–273.

[46] Jamal, M., M. Bilal, I. Ahmad, and S. Jalali-Asadabadi. IRelast package. *Journal of Alloys and Compounds*, Vol. 735, 2018, pp. 569–579.
[47] Moruzzi, V. L., J. F. Janak, and K. Schwarz. Calculated thermal properties of metals. *Physical Review B*, Vol. 37, 1988, id. 790.
[48] Moussali, A., M. B. Amina, B. Fassi, I. Ameri, M. Ameri, and Y. Al-Douri. First-principles calculations to investigate structural and thermodynamic properties of Ni2LaZ (Z = As, Sb and Bi) Heusler alloys. *Indian Journal of Physics and Proceedings of the Indian Association for the Cultivation of Science*, Vol. 94, 2020, pp. 1733–1747.
[49] Katsura, T. and Y. Tange. A simple derivation of the Birch–Murnaghan equations of state (EOSs) and comparison with EOSs derived from other definitions of finite strain. *Minerals*, Vol. 9, 2019, pp. 1–19.
[50] Khanzadeh, M. and G. Alahyarizadeh. A DFT study on pressure dependency of TiC and ZrC properties: Interconnecting elastic constants, thermodynamic, and mechanical properties. *Ceramics International*, Vol. 47, 2021, pp. 9990–10005.
[51] Khatun, M. R., M. A. Ali, F. Parvin, and A. Islam. Elastic, thermodynamic and optical behavior of V2AC (A = Al, Ga) MAX phases. *Results in Physics*, Vol. 7, 2017, pp. 3634–3639.
[52] Qin, M., J. Gild, C. Hu, H. Wang, M. S. Bin Hoque, J. L. Braun, et al. Dual-phase high-entropy ultra-high temperature ceramics. *Journal of the European Ceramic Society*, Vol. 40, 2020, pp. 5037–5050.
[53] Ma, D., B. Grabowski, F. Körmann, J. Neugebauer, and D. Raabe. Ab initio thermodynamics of the CoCrFeMnNi high entropy alloy: Importance of entropy contributions beyond the configurational one. *Acta Materialia*, Vol. 100, 2015, pp. 90–97.
[54] Singh, R.P. First principle study of structural, electronic and thermodynamic behavior of ternary intermetallic compound: CeMgTl. *Journal of Magnesium and Alloys*, Vol. 2, 2014, pp. 349–356.
[55] Bao, W., D. Liu, and Y. Duan. A first-principles prediction of anisotropic elasticity and thermal properties of potential superhard WB3. *Ceramics International*, Vol. 44, 2018, pp. 14053–14062.
[56] Fan, Q., Q. Wei, H. Yan, M. Zhang, Z. Zhang, J. Zhang, et al. Elastic and electronic properties of Pbca-BN: First-principles calculations. *Computational Materials Science*, Vol. 85, 2014, pp. 80–87.
[57] Huang, H., W. Wang, Q. Yuan, X. Rao, Y. Jing, G. Yi, et al. Pressure-dependence of mechanical and thermodynamic properties of Al_3Zr in Al–Li alloys from first-principles calculations. *Philosophical Magazine*, Vol. 99, 2019, pp. 971–991.
[58] Kim, J., H. Kwon, B. Kim, and Y. J. Suh. Finite temperature thermal expansion and elastic properties of $(Hf_{1-x}Ta_x)$ C ultra-high temperature ceramics. *Ceramics International*, Vol. 45, 2019, pp. 10805–10809.
[59] Hadi, M. A., M. Roknuzzaman, A. Chroneos, S. H. Naqib, A. K. M. A. Islam, R. V. Vovk, et al. Elastic and thermodynamic properties of new $(Zr_{3-x}Ti_x)AlC_2$ MAX-phase solid solutions. *Computational Materials Science*, Vol. 137, 2017, pp. 318–326.
[60] Xiang, H., Z. Feng, and Y. Zhou. Ab initio computations of electronic, mechanical, lattice dynamical and thermal properties of ZrP_2O_7. *Journal of the European Ceramic Society*, Vol. 34, 2014, pp. 1809–1818.
[61] Duff, A. I., T. Davey, D. Korbmacher, A. Glensk, B. Grabowski, J. Neugebauer, et al. Improved method of calculating ab initio high-temperature thermodynamic properties with application to ZrC. *Physical Review B*, Vol. 91, 2015, id. 214311.
[62] Benmakhlouf, A., A. Benmakhlouf, O. Allaoui, and S. Daoud. Theoretical study of elastic and thermodynamic properties of CuSc intermetallic compound under high pressure. *Chinese Journal of Physics*, Vol. 57, 2019, pp. 179–188.
[63] Li, Y., W. Wang, B. Zhu, M. Xu, J. Zhu, Y. Hao, et al. Elastic and thermodynamic properties of TiC from first-principles calculations. *Science China Physics, Mechanics and Astronomy*, Vol. 54, 2011, pp. 2196–2201.
[64] Stacey, F. D. and J. H. Hodgkinson. Thermodynamics with the Grüneisen parameter: Fundamentals and applications to high pressure physics and geophysics. *Physics of the Earth and Planetary Interiors*, Vol. 286, 2019, pp. 42–68.
[65] Zhou, Y., W. G. Fahrenholtz, J. Graham, and G. E. Hilmas. From thermal conductive to thermal insulating: Effect of carbon vacancy content on lattice thermal conductivity of ZrCx. *Journal of Materials Science & Technology*, Vol. 82, 2021, pp. 105–113.
[66] Hasan, M. Z., M. M. Hossain, M. S. Islam, F. Parvin, and A. Islam. Elastic, thermodynamic, electronic and optical properties of U_2Ti. *Computational Materials Science*, Vol. 63, 2012, pp. 256–260.
[67] Pogrebnjak, A. D., A. A. Bagdasaryan, I. V. Yakushchenko, and V. M. Beresnev. The structure and properties of high-entropy alloys and nitride coatings based on them. *Russian Chemical Reviews*, Vol. 83, 2014, id. 1027.
[68] Hao, A., X. Yang, X. Wang, Y. Zhu, X. Liu, and R. Liu. First-principles investigations on electronic, elastic and optical properties of XC (X = Si, Ge, and Sn) under high pressure. *Journal of Applied Physics*, Vol. 108, 2010, id. 63531.
[69] Rathod, N., S. K. Gupta, S. Shinde, and P. K. Jha. First-principles investigation of thermophysical properties of cubic ZrC under high pressure. *International Journal of Thermophysics*, Vol. 34, 2013, pp. 2019–2026.
[70] Chandra, S. A comparative study of second and third order Grüneisen parameter for solids. *Computational Condensed Matter*, Vol. 27, 2021, id. e00556.
[71] Pandey, B. K., A. K. Pandey, and C. K. Singh. Theoretical prediction of thermal pressure for solids. *AIP Conference Proceedings*, Vol. 1447, 2012, pp. 115–116.
[72] Miao, S. Q., H. P. Li, and G. Chen. Temperature dependence of thermal diffusivity, specific heat capacity, and thermal conductivity for several types of rocks. *Journal of Thermal Analysis and Calorimetry*, Vol. 115, 2014, pp. 1057–1063.
[73] Singh, P. K. Pressure dependence of bulk modulus for solids based on the first-principles results. Indian Journal of Pure & Applied Physics, Vol. 49, No. 12, 2011, pp. 829–832.
[74] Ganguly, J. *Thermodynamics in earth and planetary sciences*, Springer-Verlag, Berlin, Heidelberg, 2008.
[75] Angel, R. J., F. Miozzi, and M. Alvaro. Limits to the validity of thermal-pressure equations of state. *Minerals*, Vol. 9, 2019, id. 562.
[76] Kim, J., H. Kwon, J.-H. Kim, K.-M. Roh, D. Shin, and H. D. Jang. Elastic and electronic properties of partially ordered and disordered Zr $(C_{1-x}N_x)$ solid solution compounds: a first principles calculation study. *Journal of Alloys and Compounds*, Vol. 619, 2015, pp. 788–793.

[77] Ivashchenko, V. I., P. E. A. Turchi, and V. I. Shevchenko. First-principles study of elastic and stability properties of ZrC–ZrN and ZrC–TiC alloys. *Journal of Physics: Condensed Matter*, Vol. 21, 2009, id. 395503.
[78] Srivastava, A. and B. D. Diwan. Structural and elastic properties of ZrN and HfN: ab initio study. *Canadian Journal of Physics*, Vol. 92, 2014, pp. 1058–1061.
[79] Arya, A. and E. A. Carter. Structure, bonding, and adhesion at the ZrC (1 0 0)/Fe (1 1 0) interface from first principles. *Surface Science*, Vol. 560, 2004, pp. 103–120.
[80] Fu, H., W. Peng, and T. Gao. Structural and elastic properties of ZrC under high pressure. *Materials Chemistry and Physics*, Vol. 115, 2009, pp. 789–794.
[81] Chen, X.-J., V. V. Struzhkin, Z. Wu, M. Somayazulu, J. Qian, S. Kung, et al. Hard superconducting nitrides. *Proceedings of the National Academy of Sciences*, Vol. 102, 2005, pp. 3198–3201.
[82] Ali, M. A., M. M. Hossain, M. A. Hossain, M. T. Nasir, M. M. Uddin, M. Z. Hasan, et al. Recently synthesized $(Zr_{1-x}Ti_x)_2AlC$ $(0 \leq x \leq 1)$ solid solutions: Theoretical study of the effects of M mixing on physical properties. *Journal of Alloys and Compounds*, Vol. 743, 2018, pp. 146–154.
[83] Huang, D., Q. Liu, Y. Zhang, C. Ye, S. Zhu, Z. Fan, et al. Ablation behavior and thermal conduction mechanism of 3D ZrC–SiC-modified carbon/carbon composite having high thermal conductivity using mesophase-pitch-based carbon fibers and pyrocarbon as heat transfer channels. *Composites Part B: Engineering*, Vol. 224, 2021, id. 109201.
[84] Ali, M. A. and M. W. Qureshi. DFT insights into the new Hf-based chalcogenide MAX phase Hf2SeC. *Vacuum*, Vol. 201, 2022, id. 111072.
[85] Ali, M. A., M. M. Hossain, M. M. Uddin, A. K.M. A. Islam, and S. H. Naqib. Understanding the improvement of thermo-mechanical and optical properties of 212 MAX phase borides Zr2AB2 (A = In, Tl). *Journal of Materials Research and Technology*, Vol. 15, 2021, pp. 2227–2241.
[86] Ali, M. A. and M. W. Qureshi. Newly synthesized MAX phase Zr 2 SeC: DFT insights into physical properties towards possible applications. *RSC Advances*, Vol. 11, 2021, pp. 16892–16905.
[87] Abdollahi, A. First-principle calculations of thermodynamic properties of ZrC and ZrN at high pressures and high temperatures. *Physica B: Condensed Matter*, Vol. 410, 2013, pp. 57–62.
[88] Khanzadeh, M., H. Alipour, A. Hamedani, G. Alahyarizadeh, and M. Aghaei Moghanloo. Investigation of thermal properties of titanium carbide and zirconium carbide as a function of temperature and pressure using density functional theory. *Journal of Advanced Materials and Technologies*, Vol. 10, 2022, pp. 115–126.
[89] Li, C. M., S. M. Zeng, Z. Q. Chen, N. P. Cheng, and T. X. Chen. First-principles calculations of elastic and thermodynamic properties of the four main intermetallic phases in Al–Zn–Mg–Cu alloys. *Computational Materials Science*, Vol. 93, 2014, pp. 210–220.
[90] Cheng, H.-C., C.-F. Yu, and W.-H. Chen. First-principles density functional calculation of mechanical, thermodynamic and electronic properties of CuIn and Cu_2In crystals. *Journal of Alloys and Compounds*, Vol. 546, 2013, pp. 286–295.
[91] Bao, L., Z. Kong, D. Qu, and Y. Duan. The mechanical and thermodynamic properties of ZrTM (TM = Fe, Ru and Os) intermetallics under pressure and temperature: A first-principles predictions. *Journal of Physics and Chemistry of Solids*, Vol. 142, 2020, id. 109465.
[92] Hattabi, I., A. Abdiche, S. H. Naqib, and R. Khenata. First-principles calculations of elastic and thermodynamic properties under hydrostatic pressure of cubic InN_xP_{1-x} ternary alloys. *Chinese Journal of Physics*, Vol. 59, 2019, pp. 449–464.